nature chemistry

ARTICLES

https://doi.org/10.1038/s41557-018-0171-z

# Identification of the strong Brønsted acid site in a metal–organic framework solid acid catalyst

Christopher A. Trickett[1,2,6], Thomas M. Osborn Popp[1,2,3,6], Ji Su[1,2], Chang Yan[4], Jonathan Weisberg[1], Ashfia Huq[5], Philipp Urban[1,2], Juncong Jiang[1,2], Markus J. Kalmutzki[1,2], Qingni Liu[1,2], Jayeon Baek[1,2], Martin P. Head-Gordon[1], Gabor A. Somorjai[1,2], Jeffrey A. Reimer[2,3] and Omar M. Yaghi[1,2]*

**It remains difficult to understand the surface of solid acid catalysts at the molecular level, despite their importance for industrial catalytic applications. A sulfated zirconium-based metal–organic framework, MOF-808-$SO_4$, was previously shown to be a strong solid Brønsted acid material. In this report, we probe the origin of its acidity through an array of spectroscopic, crystallographic and computational characterization techniques. The strongest Brønsted acid site is shown to consist of a specific arrangement of adsorbed water and sulfate moieties on the zirconium clusters. When a water molecule adsorbs to one zirconium atom, it participates in a hydrogen bond with a sulfate moiety that is chelated to a neighbouring zirconium atom; this motif, in turn, results in the presence of a strongly acidic proton. On dehydration, the material loses its acidity. The hydrated sulfated MOF exhibits a good catalytic performance for the dimerization of isobutene (2-methyl-1-propene), and achieves a 100% selectivity for C8 products with a good conversion efficiency.**

The chemistry at the surface of solid acid catalysts is of vital importance for industrial catalytic applications, yet a precise molecular picture of these surfaces remains elusive. Attempts to obtain a clear view of the Brønsted acid sites in solid acids such as sulfated zirconia have resulted in multiple proposed models, in part due to the difficulty in characterizing the surface structures of these materials, but also because of wildly variable properties that depend on the preparation conditions[1–11]. Discerning the molecular structures responsible for the activity of solid acid catalysts provides a richer perspective on the functional properties and catalytic mechanisms of these materials, and illuminates the fundamental surface chemistry that relates the molecular structures and their functions. Recently, the synthesis of a metal–organic framework (MOF) solid acid catalyst was reported, achieved by treating a Zr-based MOF, MOF-808, with sulfuric acid to yield the solid acid MOF, MOF-808-$SO_4$, which was shown to be capable of performing several acid-catalysed reactions[12,13]. In this report, we conclusively identify the structure of the strong Brønsted acid site in MOF-808-$SO_4$ as a hydrogen bond pair of two species, water and chelating sulfate, adsorbed on the surface of its zirconium clusters, where the acidic proton arises as a result of the hydrogen bond. We achieved this through a union of crystallographic, spectroscopic and computational studies. We also show that MOF-808-$SO_4$ exhibits good activity and selectivity for the dimerization of isobutene to isooctene, and that dehydration of the material significantly reduces the catalytic activity, which confirms the role of water as necessary to the strong acidity of the site.

## Results and discussion

The preparation of MOF-808-$SO_4$ was performed by first synthesizing pristine MOF-808 (Fig. 1a), $Zr_6O_5(OH)_3(BTC)_2(HCOO)_5(OH_2)_2$ (BTC, benzenetricarboxylate), with a subsequent exchange of the formate ions on the zirconium clusters for sulfate ions simply by washing the MOF in dilute sulfuric acid[12,14]. The MOF-808 backbone comprises an octahedron of zirconium atoms that are triply bridged by $\mu^3$-O and $\mu^3$-OH groups. The formate groups in the pristine structure each bridge two zirconium atoms to form a six-membered belt around the cluster[13]. One cluster is connected to six other clusters through BTC linkers, three above and three below the belt of formates, which results in a framework with spn topology. Once the formate ions are exchanged for sulfate to yield MOF-808-$SO_4$ (Fig. 1b), these sulfates may take on multiple binding modes and can take one of several positions along the belt interspersed between additional ligated water molecules, which results in long-range disorder from one cluster to the next. As this disorder is confined to the surface species on the zirconium clusters, the surface of each cluster has a slightly different local molecular 'decoration' (Fig. 1c), whereas the structural backbone of MOF-808 is still conserved throughout[15–18]. Our challenge is to understand the molecular decoration of the zirconium clusters in MOF-808-$SO_4$ by first identifying the structures that decorate the cluster surface, and from there, discerning which arrangement of decorating structures results in a strong Brønsted acid site.

**Understanding the molecular decoration of the zirconium clusters.** To elucidate the coordination mode of sulfate is essential to discern the local structures that exist on the surface of the clusters. Single-crystal X-ray diffraction analysis of a crystal in aqueous solution showed that the sulfate groups are coordinated in both a bridging and chelating mode (Supplementary Fig. 1), with the bridging mode dominating in a 4:1 ratio over the chelating one (Supplementary Section 3). To obtain further insight into

[1]Department of Chemistry, Kavli Energy NanoSciences Institute at Berkeley, and Berkeley Global Science Institute, University of California-Berkeley, Berkeley, California, USA. [2]Materials Sciences Division, Lawrence Berkeley National Laboratory, Berkeley, CA, USA. [3]Department of Chemical and Biomolecular Engineering, University of California, Berkeley, California, USA. [4]Department of Chemistry, Stanford University, Stanford, CA, USA. [5]Neutron Scattering Division, Oak Ridge National Laboratory, Oak Ridge, TN, USA. [6]These authors contributed equally: Christopher A. Trickett, Thomas M. Osborn Popp *e-mail: yaghi@berkeley.edu

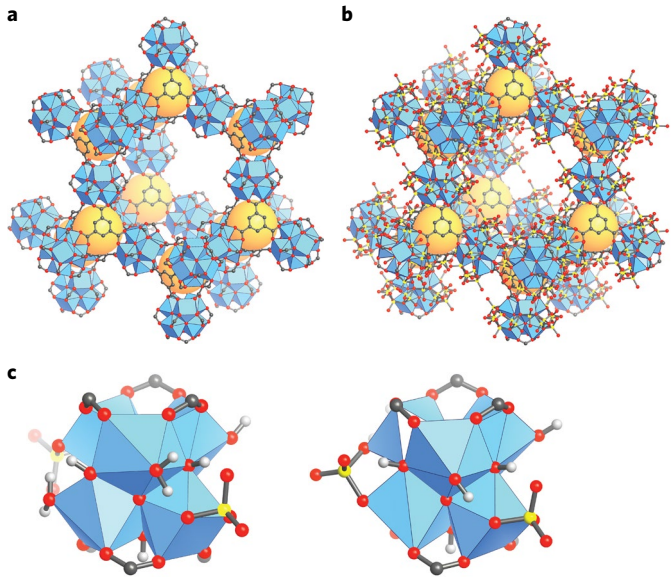


**Fig. 1 | MOF-808, MOF-808-$SO_4$ and visualization of differences in molecular decoration. a**, Pristine MOF-808 comprises six connected zirconium-based metal clusters that contain five formate groups and are linked by BTC into the depicted spn topology framework. **b**, These formates may be substituted with sulfate anions, which coordinate in a bidentate fashion to zirconium, either in a chelating mode to a single zirconium atom, or in a bridging mode to two zirconium atoms. Sulfate is predominantly in the bridging mode in the solvated MOF, and converts exclusively to the chelating mode after activation by heating under a dynamic vacuum. **c**, Two representations of the modelled zirconium clusters, with BTC linkers omitted beyond the coordinating carboxylate group, highlight the differences in molecular decoration between different clusters in the overall structure. A similar stoichiometry of hydroxide, water and sulfate groups are present on each cluster, but the local arrangement and apportionment of these groups differ. Zr-based clusters ($Zr_6O_5(OH)_3$), blue polyhedra; O, red; C, grey; S, yellow; H, white; pores, large yellow spheres. In **a** and **b**, hydrogen atoms are omitted for clarity. a.u., arbitrary units.

what factors control the coordination mode of these ions, selenated MOF-808 (MOF-808-$SeO_4$) was synthesized in a similar manner to sulfated MOF-808. The MOF-808-$SeO_4$ framework in aqueous solution was found to possess only one coordination mode for selenate, in which selenate bridges two zirconium atoms, which suggests that perhaps the increased atomic radius of selenium enforces the bridging coordination mode. However, on activation of these two MOFs under a dynamic vacuum and heating at 120 °C, both sulfate and selenate were found to have shifted exclusively into the chelating mode. This was confirmed using a Rietveld refinement of the samples measured by powder X-ray diffraction (PXRD) in an argon atmosphere. The solid acid nature of MOF-808-$SO_4$ is only observed after activation at 120 °C, which suggests that the chelating coordination mode of sulfate is a key contributor to its catalytic activity.

Quantifying the average molecular formula for MOF-808-$SO_4$ constrains further the possibilities for ligand disorder on the surface of the zirconium clusters. Here, balancing the charge on the zirconium clusters guides our stoichiometric analysis. Using inductively coupled plasma–optical emission spectroscopy for elemental analysis, 2.3 sulfur atoms per 6 zirconium atoms were found, so an average of 2.3 sulfate groups per zirconium cluster. As each zirconium atom is in the +4 oxidation state, there is an excess of positive charge that is not properly accounted for within the model so far. To probe this, we turned to powder neutron diffraction (PND) to obtain more precise information on the occupancies and thermal ellipsoids of light elements within the framework (Fig. 2a). A sample of MOF-808-$SO_4$ with a deuterated BTC linker was measured at 10 K and 300 K and refined simultaneously against a structure model, which revealed a 1:1 ratio of $\mu^3$-O to $\mu^3$-OH in both independent crystallographic positions within two standard deviations (Supplementary Section 2). An excess of $\mu^3$-O is therefore not what balances the excess positive charge. Substantially more electron density is located around the position of the oxygen that connects zirconium to sulfur, O6, which is the same location as the coordinated water molecules bound to the cluster in the as-synthesized MOF-808-$SO_4$. Note that the sulfate position could not be located by PND due to the low occupancy and extremely weak neutron scattering factor of sulfur, and thus information from PXRD was used in combination with elemental analysis to confirm its presence in this sample.

As the only electron density unaccounted for in this model is located at position O6, where water is present in the structure prior to activation, we can infer that the balance of the excess positive charge is achieved here by a terminal hydroxide, produced by the deprotonation of water molecules. This assumption is plausible given that terminal water molecules bound to zirconium hydroxide clusters have been found to be acidic[19,20]. The position thus accounts for the crystallographically superimposed oxygen from sulfate groups, hydroxide and water molecules that were not removed during the activation process. This overlap excludes the possibility of determining the precise coordinates of the hydroxide, water and sulfate oxygen, but the total occupancy of these species was refined freely, and converged to 78.4 ± 1.1%. This corresponds to 9.4 oxygen atoms per cluster, out of a possible 12. As there must be 4.6 oxygen atoms from 2.3 bidentate sulfate groups, as found by elemental analysis, and 1.4 hydroxide groups for charge balancing, this leaves 3.4 ± 0.1 oxygen atoms unaccounted for, and so are assigned to ligated water. This was confirmed by thermogravimetric analysis–mass spectrometry on the activated sample, which demonstrated the loss of 3.1 water molecules per cluster prior to structure decomposition (Supplementary Fig. 16). The first water signal observed from the mass spectrometer peaked at 143 °C, which indicates water is still present after evacuation and heating. After a small, second water-loss event at 236 °C, the structure decomposes at around 350 °C. This trend can be explained by considering that the loss of neutral terminal water ligands would not collapse the structure, but once the framework is completely dehydrated any further mass loss leads to structure decomposition, as this involves the loss of charged species. Evidence from elemental analysis, PND, $^1$H NMR spectroscopy of the digested MOF and thermogravimetric analysis–mass spectrometry, led to an average molecular formula of $Zr_6O_4(OH)_4(BTC)_2(SO_4)_{2.3}(OH)_{1.4}(OH_2)_{3.1}(DMF)_{0.4}$ (DMF, dimethylformamide) for the activated form of MOF-808-$SO_4$.

**Identifying the strong Brønsted acid site.** With the average chemical formula now known, the possible species that decorate each zirconium cluster are constrained, which simplifies the task of identifying the Brønsted acid site in MOF-808-$SO_4$. The potential acidic sources are discussed in turn. First, terminal hydroxide may be eliminated simply because terminal water is present and bound to the cluster in the same manner as the hydroxide, with terminal water being known to be more acidic[18,19]. Protons on the sulfate can also be ruled out because the pH of the solution when the MOF is washed with water after incorporation of the sulfate is 3.5, whereas the $pK_{a2}$ value of sulfuric acid is 1.92 (ref. [21]). Therefore, sulfate must be fully deprotonated at this stage. A direct comparison between $\mu^3$-OH and terminal water is not as straightforward; however, we found that the water molecules bound to the framework could be successfully removed by holding the temperature at 220 °C overnight with the crystallinity and porosity maintained. Hereafter, this sample is referred to as dehydrated MOF-808-$SO_4$. If the water molecules are,

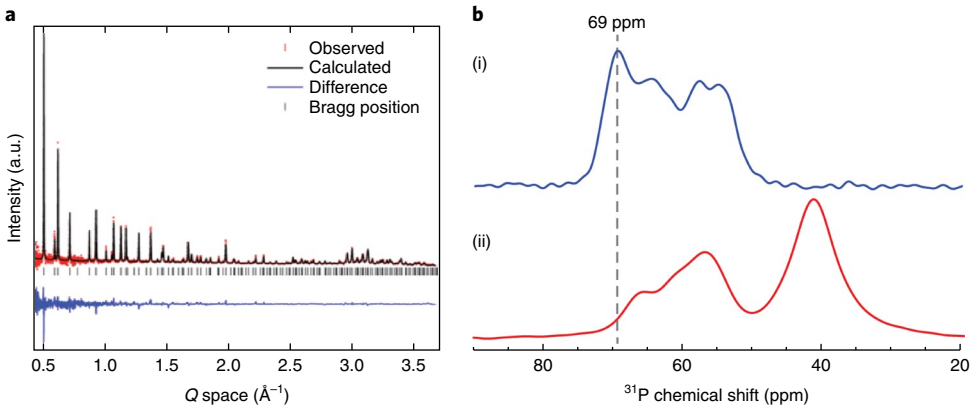


**Fig. 2 | Structural characterization of MOF-808-$SO_4$ by a Rietveld refinement of powder neutron data, and NMR evidence for the presence of water being central to the strong acid site. a**, The data obtained from PND is compared against the calculated pattern from the structural model and their difference. *R* factors in the Rietveld refinement: $R_{wp}=2.91\%$, $R_p=9.59\%$. **b**, $^{31}$P MAS solid-state NMR spectra of TMPO adsorbed into MOF-808-$SO_4$ (blue) (**i**) and dehydrated MOF-808-$SO_4$ (red) (**ii**). The peak at 69 ppm, assigned to TMPO interacting with the strong Brønsted acid site, is lost on dehydration. The peak centred at 42 ppm is due to excess TMPO that does not interact with acid sites directly. Other peaks in the spectra belong to TMPO adsorbed at various $\mu^1$-OH, $\mu^3$-OH and terminal water sites.

indeed, the most acidic species present, the material should lose its strong acid properties on dehydration.

To determine if water molecules are the source of the most acidic protons, we adsorbed trimethylphosphine oxide (TMPO) into MOF-808-$SO_4$ as a probe of acidity and performed $^{31}$P magic-angle-spinning (MAS) solid-state NMR spectroscopy. TMPO interacts with Brønsted and Lewis acid sites via the lone pairs on its oxygen atom. Strong acid sites polarize the phosphorus–oxygen bond, which results in a linear relationship between the $^{31}$P chemical shift values of adsorbed TMPO and the strength of the acid site, where a higher $^{31}$P chemical shift corresponds to a stronger acid site[22–26]. MOF-808-$SO_4$ with adsorbed TMPO showed a $^{31}$P resonance at 69 ppm associated with a strongly acidic site (Fig. 2b,i), consistent with previous observations for this material[12]. This resonance at 69 ppm was found to be absent when TMPO was used in dehydrated MOF-808-$SO_4$ (Fig. 2b,ii). As the loss of a water molecule is associated with the loss of the strongest acid site, this result supports the role of terminal water as the strongest Brønsted acid source.

At this point, two key molecular features that decorate the zirconium clusters are now identified as essential to the acidity of MOF-808-$SO_4$: the chelating mode of sulfate and terminal water ligand. In isolation, neither of these two species is sufficient to account for the acidity of this MOF, and therefore its strong Brønsted acidity must arise from a specific arrangement of these species on the cluster surface. Given the many possible ways to decorate the belt of the cluster with terminal water, terminal hydroxide and chelating sulfate, several arrangements were chosen to be modelled and geometrically optimized using density functional theory (DFT). The formula $Zr_6O_4(OH)_4(C_2H_3O_2)_6(SO_4)_2(OH)_2(OH_2)_x$ was used as a representation of an average cluster, where $x=2$ or 3. The restrictions on the structural arrangement of the cluster included (1) the core $[Zr_6O_4(OH)_4(C_2H_3O_2)_6]^{6+}$ being fixed with the $\mu^3$-O and –OH groups arranged in the commonly reported alternating arrangement to minimize charge repulsion, (2) modelling sulfate as chelating to zirconium as opposed to bridging, (3) using a terminal hydroxide to charge balance the cluster and (4) including 2–3 water molecules per cluster. Additionally, individual clusters were modelled by truncating the linker with acetate groups, which assumes the clusters are electronically decoupled. The most enlightening result obtained from the different modelled arrangements on the clusters is from the comparison of terminal water in isolation versus one adjacent to a chelating sulfate group. An O–H bond length of 0.98 Å was observed on the terminal water molecules that have no significant interactions with neighbouring adsorbed molecules. However, when the terminal water molecule was adjacent to a chelating sulfate, there was a strong hydrogen bond interaction, with an O–H bond length that ranged from 1.02 to 1.05 Å, depending on the particular cluster modelled, significantly longer than the O–H bond with no hydrogen bonding. This was accompanied by an O–H···O angle of 163–166° and a short H···O hydrogen bonding distance of 1.50–1.66 Å, which indicates that the proton was very weakly bound. Indeed, the system can be viewed as a protonated conjugate of an adsorbed pair of hydroxide and sulfate, with the proton sitting between the two groups, but localized mostly on the hydroxide. One example of this site on a modelled cluster is represented in Fig. 3, which was modelled with overall two water molecules and two chelating sulfate groups located on opposite sides of the zirconium cluster.

The broken symmetry of the water molecule at this proposed acid site implies that the water participating in a hydrogen bond to a chelating sulfate should have distinctly different spectroscopic signatures for its two proton environments. We refer to these two sites as $H_a$ for the acidic proton on water that participates in the hydrogen bond to the chelating sulfate, and $H_b$ for the other proton that points into free space. To probe these proton chemical environments directly, we performed $^1$H solid-state NMR. Figure 4a shows the $^1$H MAS NMR spectrum of MOF-808-$SO_4$ at 6 kHz MAS taken before and after dehydration, and their difference. The difference spectrum shows that two peaks at around 2.5 ppm and 8.1 ppm are lost as a result of dehydration. Assigning the identity of these resonances is informed by comparison with the DFT-calculated $^1$H NMR chemical shifts of two of the modelled zirconium clusters (Supplementary Section 7 and Supplementary Tables 4 and 5). The difference in chemical shift ($\Delta\delta$) between the $H_a$ and $H_b$ protons in the acid site is calculated for the two cases to be $\Delta\delta=5.1$ and 9.1 ppm, respectively. Water that lacks a strong hydrogen bonding interaction to the chelating sulfate is calculated to have only $\Delta\delta=2.0$ ppm between the two protons. The changes in the spectra in Fig. 4a after dehydration suggest that the two lost resonances belong to the $H_a$ and $H_b$ protons on the water molecule in the acid site with $\Delta\delta=5.6$ ppm, where $H_a$, the acidic proton, is the downfield resonance.

To confirm that these two resonances are the $H_a$ and $H_b$ protons that belong to the same water molecule, a rotor-synchronized double-quantum (DQ) MAS NMR experiment with a back-to-back recoupling sequence was performed. This experiment correlates

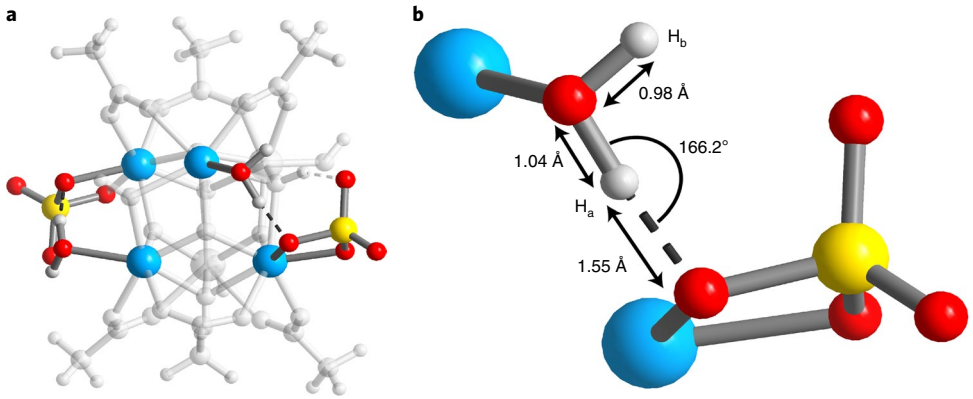


**Fig. 3 | Depiction of the zirconium cluster and Brønsted acid site in MOF-808-$SO_4$ as determined by DFT geometry optimization. a**, The overall cluster. **b**, A close-up view of the acid site with the relevant bond lengths and angles, and with the acidic proton that participates in the hydrogen bond labelled as $H_a$ and the other as $H_b$. Zr, blue; O, red; S, yellow; H, white; atoms not directly part of the active site are in light grey.

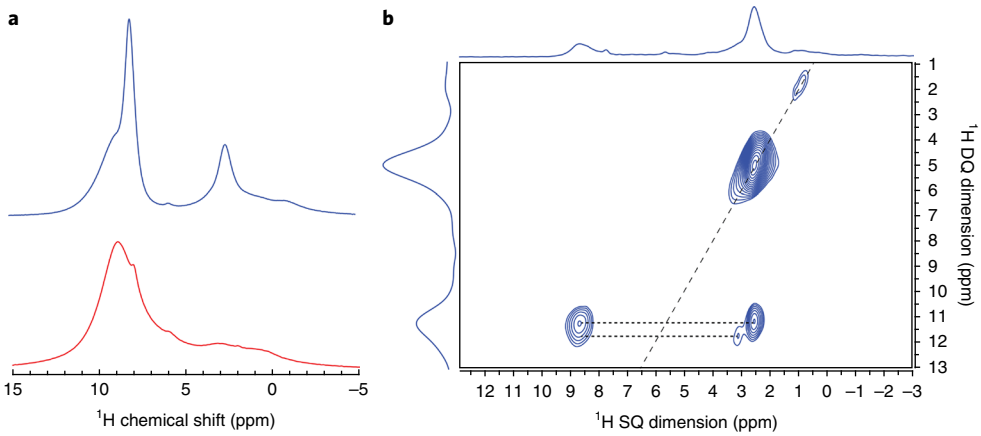


**Fig. 4 | Identification of the resonances attributable to adsorbed water using $^1$H solid-state NMR, comparing MOF-808-$SO_4$ before and after dehydration. a**, The $^1$H MAS NMR spectrum of MOF-808-$SO_4$ at 6 kHz MAS (blue) and the $^1$H MAS NMR spectrum of dehydrated MOF-808-$SO_4$ at 6 kHz MAS (red) show the loss of two prominent peaks assigned to the two inequivalent protons on a water molecule hydrogen-bonded to sulfate. **b**, $^1$H DQ-MAS NMR spectrum of MOF-808-$SO_4$ with SQ and DQ skyline projections (blue). The spectrum was recorded at 12.5 kHz with two cycles of the back-to-back recoupling sequence for excitation and reconversion of the DQ coherence. The two peaks that are lost on dehydration appear at 2.5 and 8.7 ppm and exhibit a DQ coherence at 11.2 ppm, and are assigned as the inequivalent protons on the terminal water hydrogen bonded to a chelating sulfate. The prominent peak along the autocorrelation diagonal at 5 ppm is assigned as a terminal water elsewhere on the zirconium cluster, not adjacent to a sulfate.

proton resonances in the standard single-quantum (SQ) spectrum by their proximity to one another through space. A peak in the DQ dimension indicates that a pair of protons is in close enough proximity to generate a double quantum coherence[27]. As the closest pairs of protons in MOF-808-$SO_4$ belong to those on $\mu^1$-water molecules, we expect these to be the primary coherences observed. The intensity of these peaks is dependent on the number of duplicate pairs that exhibit this coherence as well as the efficiency at which this coherence is excited, that is, the internuclear distance[28]. The SQ $H_a$ and $H_b$ resonances at 8.7 and 2.5 ppm, respectively, exhibit strong cross peaks at a DQ frequency of 11.2 ppm, which indicates their close spatial proximity and confirms that these two resonances must arise from a single water species (Fig. 4b). The low-intensity cross peaks between 8.7 and 3.1 ppm may arise from a small subset of $H_a$ and $H_b$ protons in acid sites with a slightly different local arrangement of nearest-neighbour $\mu^1$-OH and $\mu^3$-OH groups. Along the diagonal, a strong autocorrelation DQ peak at around 5.0 ppm is observed for an SQ resonance at around 2.5 ppm, which arises from pairs of protons that belong to isolated terminal water at other sites on the zirconium cluster. The chemical environment of the protons on water molecules that do not neighbour a chelating sulfate is similar to the chemical environment of the $H_b$ proton in the acid site and, accordingly, their chemical shifts should be similar. This is supported by our DFT calculations, in which the chemical shifts of protons in these environments were calculated to be within about ±1 ppm of one another. The $^1$H solid-state NMR results reveal a picture consistent with the proposed molecular conformation of the Brønsted acid site, in which water hydrogen bonded to sulfate has two protons with inequivalent O–H bond lengths and inequivalent chemical shifts. The subsequent loss of these peaks after dehydration at 220 °C is correlated with a loss of acidity, which results in the conclusion that the strong Brønsted acid site arises from this hydrogen-bonding interaction between water and a chelating sulfate.

**Removal of water at the acid site impacts catalytic performance.** These results suggest a structure–property relationship in MOF-808-$SO_4$, where water must be present and adjacent to a chelating sulfate to yield a strong acidity. We sought to test this hypothesis by measuring the activity of MOF-808-$SO_4$ in catalysing the dimerization of isobutene (2-methyl-1-propene), and to see whether

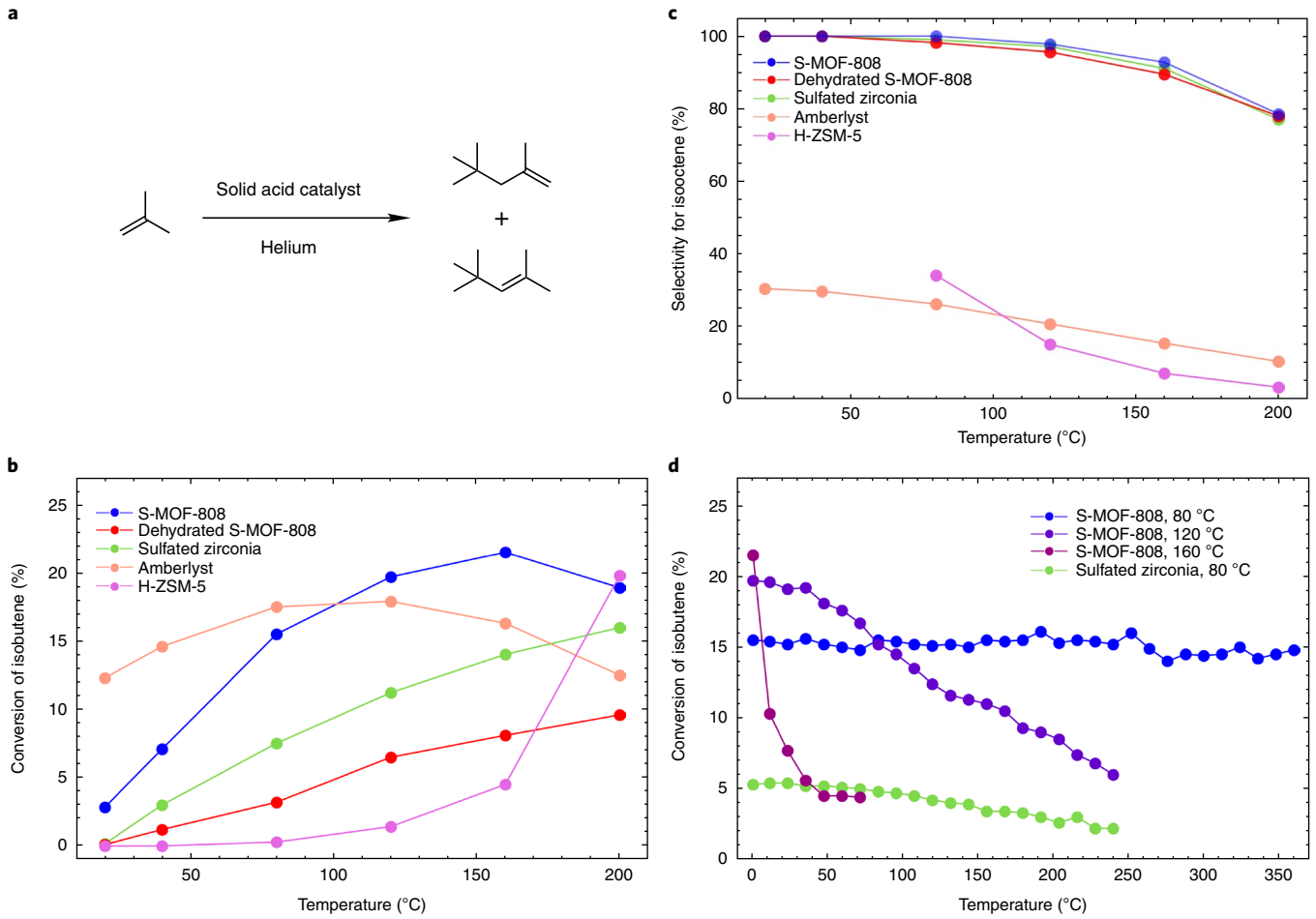


**Fig. 5 | Comparison of the catalytic conversion, selectivity and long-term stability of MOF-808-$SO_4$ and dehydrated MOF-808-$SO_4$ against benchmark catalysts. a**, General reaction scheme for the dimerization of isobutene (2-methyl-1-propene) to isooctene (2,4,4-trimethyl-1-pentene and 2,4,4-trimethyl-2-pentene). **b**, Plot of the percent conversion of isobutene into isooctene for MOF-808-$SO_4$, dehydrated MOF-808-$SO_4$, sulfated zirconia, Amberlyst and H-ZSM-5 from room temperature up to 200 °C. Amberlyst is the most active at low temperatures, whereas MOF-808-$SO_4$ has a strong temperature dependence. Dehydrated MOF-808-$SO_4$ has a significantly lower conversion efficiency, which indicates that the presence of water adjacent to a chelating sulfate is responsible for the majority of the activity. **c**, Plot of the selectivity for dimer products over higher-order oligomers. Both Amberlyst and H-ZSM-5 have poor selectivity and favour higher-order oligomers at all temperatures. MOF-808-$SO_4$, dehydrated MOF-808-$SO_4$ and sulfated zirconia have a nearly 100% selectivity for dimer products up to 80 °C. **d**, Plot of the long-term catalytic performance of MOF-808-$SO_4$ for the dimerization of isobutene at 80 °C, 120 °C and 160 °C against sulfated zirconia at 80 °C. The conversion efficiency for MOF-808-$SO_4$ is maintained at 80 °C, but at higher temperatures the material loses activity with an increasing rate, probably due to desorption of the terminal water from the clusters at these temperatures. Sulfated zirconia at 80 °C has approximately one-third of the activity of MOF-808-$SO_4$ at 80 °C, but falls to about half this value by 240 h, whereas MOF-808-$SO_4$ maintains its conversion level throughout this period.

removing the water molecule in the active site by dehydration would affect this activity. The dimerization of isobutene may yield two products, either 2,4,4-trimethyl-1-pentene or 2,4,4-trimethyl-2-pentene, both referred to as isooctene (Fig. 5a). The terminal alkene product is prized as a starting material to synthesize terminal aldehydes and alcohols, but both alkene products may be hydrogenated to form 2,4,4-trimethylpentane, known as isooctane, a valuable gasoline octane booster[29–31]. In the process of dimerizing isobutene, higher-order alkene oligomer products greater than C8 may form, which is typically disfavoured, as a separation step is required to isolate the C8 species. Selectivity for C8 products is crucial if isooctane is the desired product[32,33]. To that end, MOF-808-$SO_4$ was benchmarked against other solid acid catalysts for C8 selectivity and conversion efficiency (sulfated zirconia, Amberlyst and H-ZSM-5) using a continuous gas flow set-up, with isobutene diluted in helium and at atmospheric pressure (Supplementary Section 11). The advantage of using a gas flow set-up over a solvent-based process is that it allows for continuous production, and negates the need to purify isooctene from solvent mixtures. Our benchmark materials were chosen based on their capacity to operate under these conditions, and their catalytic activities were evaluated with respect to the mass of the catalyst. MOF-808-$SO_4$ was found to be active even at room temperature, with conversion peaking at 160 °C at 21.5%, which outperformed Amberlyst, sulfated zirconia and H-ZSM-5 under these conditions (Fig. 5b). The C8 selectivity of MOF-808-$SO_4$ was 100% at 80 °C and lower, yet remained at 92.8% at 160 °C, similar to sulfated zirconia (Fig. 5c). The C8 product distribution for both MOF-808-$SO_4$ and sulfated zirconia runs at about 4:1 in favour of the terminal alkene product (Supplementary Figs. 28–30). H-ZSM-5 and Amberlyst exhibit a C8 selectivity under 35% at all temperatures, to form a mixture of many different higher-order oligomers. Although the C8 selectivity and product distribution for MOF-808-$SO_4$ and sulfated zirconia are comparable, under longer experiments of up to 15 days at 80 °C, MOF-808-$SO_4$ does not lose activity or selectivity,

maintaining a constant 15% conversion, whereas the conversion efficiency of sulfated zirconia drops by around 60% from its starting value of 5.2% (Fig. 5d). MOF-808-$SO_4$ does begin to lose activity at 120 °C and 160 °C, and at a faster rate with increasing temperature, consistent with the notion that the desorption of water from the zirconium clusters at higher temperatures should affect the Brønsted acid site. Indeed, when dehydrated MOF-808-$SO_4$ was tested as a catalyst, the conversion was 80% less than that of MOF-808-$SO_4$ at 80 °C (Fig. 5b). The great majority of the catalytic activity of the material can thus be attributed to this acid site, where water is adjacent and hydrogen bonded to the chelating sulfate. The C8 selectivity and product distribution for dehydrated MOF-808-$SO_4$ are almost identical to that of MOF-808-$SO_4$ and sulfated zirconia, which indicates that this acid site alone is not responsible for the selectivity.

We conclude that perturbing the strong Brønsted acid site by removing the water adjacent to the chelating sulfate has a significant negative impact on the catalytic performance of MOF-808-$SO_4$. The remaining activity of the material in the absence of this water molecule suggests that Lewis acid sites in the material may also contribute to its activity, but to a lesser extent, a possibility supported by the observation of open metal sites in the PND refinement of the structure (Supplementary Section 2). Regeneration of the catalyst thus only requires replacing the water molecule adjacent to the sulfate, which can be done by repeating the solvent exchange and activation process. Future work may find a more efficient process whereby the catalyst is regenerated continuously during the operation by the addition of water vapour into the product stream, and so maintain the active site even at higher temperatures.

The relative strength of this acid site compared to that of other acids is of interest, as its structure may serve as a model for the design of new strong acid sites. Although MOF-808-$SO_4$ has been previously stated to be superacidic by colorimetric methods[12], these methods can sometimes prove unreliable for acid sites that exist at the interface of the solid and gas phase[34]. We can provide a thermodynamically based estimate of the acidity of this specific Brønsted acid site based on a previously calculated relationship between the $^{31}$P chemical shift of adsorbed TMPO and the deprotonation energy of simulated Brønsted acid sites[21,22]. The TMPO resonance at 69 ppm correlated to the acid site in this material corresponds to a deprotonation energy of 1,214 kJ mol$^{-1}$. It is generally accepted that a superacid is a medium in which the chemical potential of the proton is higher than that in sulfuric acid[35]. The deprotonation energy for gas-phase sulfuric acid has been experimentally determined to be 1,295 kJ mol$^{-1}$ (ref. [36]), which suggests that this Brønsted site in MOF-808-$SO_4$ is at the very least comparable to sulfuric acid, and may even be considered superacidic by this measure. At its core, the structure of this site in MOF-808-$SO_4$ is characterized by the pairing of two bases (chelating sulfate and $\mu^1$-OH) supported on two neighbouring zirconium atoms and sharing a weakly bound proton between them. Thus, such a Brønsted acid site construct may be quite generalizable, as it may be possible to reduce the deprotonation energy of this proton to yield even stronger acidity by manipulating the identities of these two bases or of the support atoms.

## Data availability

Synthetic and experimental procedures, as well as crystallographic, spectroscopic and computational data are provided in the Supplementary Information. Crystallographic data for the structures reported in this Article have been deposited at the Cambridge Crystallographic Data Centre, under deposition numbers CCDC 1871192 (MOF-808), 1871193 (MOF-808-SO4) and 1871194 (MOF-808-SeO4). Copies of the data can be obtained free of charge via www.ccdc.cam.ac.uk/data_request/cif. All other data supporting the findings of this study are available within the article and its Supplementary Information, or from the corresponding author upon reasonable request.

Received: 13 December 2017; Accepted: 12 October 2018;
Published online: 19 November 2018

## References

1. Arata, K. Solid superacids. *Adv. Catal.* **37**, 165 (1990).
2. Ward, D. A. & Ko, E. I. One-step synthesis and characterization of zirconia–sulfate aerogels as solid superacids. *J. Catal.* **150**, 18–33 (1994).
3. Haase, F. & Sauer, J. The surface structure of sulfated zirconia: periodic ab initio study of sulfuric acid adsorbed on $ZrO_2$(101) and $ZrO_2$(001). *J. Am. Chem. Soc.* **120**, 13503–13512 (1998).
4. Bensitel, M., Saur, O., Lavalley, J. C. & Morrow, B. A. An infrared study of sulfated zirconia. *Mater. Chem. Phys.* **19**, 147–156 (1988).
5. Clearfield, A., Serrette, G. P. D. & Khazi-Syed, A. H. Nature of hydrous zirconia and sulfated hydrous zirconia. *Catal. Today* **20**, 295–312 (1994).
6. Kustov, L. M., Kazansky, V. B., Figueras, F. & Tichit, D. Investigation of the acidic properties of $ZrO_2$ modified by $SO_4^{2-}$ anions. *J. Catal.* **150**, 143–149 (1994).
7. Adeeva, V. et al. Acid sites in sulfated and metal-promoted zirconium dioxide catalysts. *J. Catal.* **151**, 364–372 (1995).
8. Bolis, V., Magnacca, G., Cerrato, G. & Morterra, C. Microcalorimetric characterization of structural and chemical heterogeneity of superacid $SO_4$/$ZrO_2$ systems. *Langmuir* **13**, 888–894 (1997).
9. Hino, M., Kurashige, M., Matsuhashi, H. & Arata, K. The surface structure of sulfated zirconia: studies of XPS and thermal analysis. *Thermochim. Acta* **441**, 35–41 (2006).
10. Arata, K. Organic syntheses catalyzed by superacidic metal oxides: sulfated zirconia and related compounds. *Green Chem.* **11**, 1719–1728 (2009).
11. Yadav, G. D. & Nair, J. J. Sulfated zirconia and its modified versions as promising catalysts for industrial processes. *Microporous Mesoporous Mater.* **33**, 1–48 (1999).
12. Jiang, J. et al. Superacidity in sulfated metal—organic framework-808. *J. Am. Chem. Soc.* **136**, 12844–12847 (2014).
13. Furukawa, H. et al. Water adsorption in porous metal–organic frameworks and related materials. *J. Am. Chem. Soc.* **136**, 4369–4381 (2014).
14. Goesten, M. G. et al. Sulfation of metal–organic frameworks: opportunities for acid catalysis and proton conductivity. *J. Catal.* **281**, 177–187 (2011).
15. Osborn Popp, T. M. & Yaghi, O. M. Sequence-dependent materials. *Acc. Chem. Res.* **50**, 532–534 (2017).
16. Cairns, A. B. & Goodwin, A. L. Structural disorder in molecular framework materials. *Chem. Soc. Rev.* **42**, 4881–4893 (2013).
17. Furukawa, H., Müller, U. & Yaghi, O. M. 'Heterogeneity within order' in metal–organic frameworks. *Angew. Chem. Int. Ed.* **54**, 3417–3430 (2015).
18. Trickett, C. A. et al. Definitive molecular level characterization of defects in UiO-66 crystals. *Angew. Chem. Int. Ed.* **54**, 11162–11167 (2015).
19. Åberg, M. & Glaser, J. $^{17}$O and $^{1}$H NMR study of the tetranuclear hydroxo zirconium complex in aqueous solution. *Inorg. Chim. Acta* **206**, 53–61 (1993).
20. Springborg, J. Hydroxo-bridged complexes of chromium (III), cobalt (III), rhodium (III), and iridium (III). *Adv. Inorg. Chem.* **32**, 55–169 (1988).
21. Hall, J. *Lab Manual for Zumdahl/Zumdahl's Chemistry* 656 (Brooks Cole, Pacific Grove, 2002).
22. Zheng, A., Zhang, H., Lu, X., Liu, S. B. & Deng, F. Theoretical predictions of $^{31}$P NMR chemical shift threshold of trimethylphosphine oxide absorbed on solid acid catalysts. *J. Phys. Chem. B* **112**, 4496–4505 (2008).
23. Zheng, A. et al. $^{31}$P chemical shift of adsorbed trialkylphosphine oxides for acidity characterization of solid acids catalysts. *J. Phys. Chem.* **112**, 7349–7356 (2008).
24. Zheng, A., Huang, S. J., Liu, S. B. & Deng, F. Acid properties of solid acid catalysts characterized by solid-state $^{31}$P NMR of adsorbed phosphorous probe molecules. *Phys. Chem. Chem. Phys.* **13**, 14889 (2011).
25. Chen, W. H. et al. A solid-state NMR, FT-IR and TPD study on acid properties of sulfated and metal-promoted zirconia: influence of promoter and sulfation treatment. *Catal. Today* **116**, 111–120 (2006).
26. Lunsford, J. H., Sang, H., Campbell, S. M., Liang, C. H. & Anthony, R. G. An NMR study of acid sites on sulfated-zirconia catalysts using trimethylphosphine as a probe. *Catal. Lett.* **27**, 305–314 (1994).
27. Gottwald, J., Demco, D. E., Graf, R. & Spiess, H. W. High-resolution double-quantum NMR spectroscopy of homonuclear spin pairs and proton connectivities in solids. *Chem. Phys. Lett.* **243**, 314–323 (1995).
28. Schnell, I., Brown, S. P., Low, H. Y., Ishida, H. & Spiess, H. W. An investigation of hydrogen bonding in benzoxazine dimers by fast magic-angle spinning and double-quantum $^{1}$H NMR spectroscopy. *J. Am. Chem. Soc.* **120**, 11784–11795 (1998).
29. Mahdi, H. I. & Muraza, O. Conversion of isobutylene to octane-booster compounds after methyl *tert*-butyl ether phaseout: the role of heterogeneous catalysis. *Ind. Eng. Chem. Res.* **55**, 11193–11210 (2016).
30. Takahashi, K., Yamashita, M. & Nozaki, K. Tandem hydroformylation/hydrogenation of alkenes to normal alcohols using Rh/Ru dual catalyst or Ru single component catalyst. *J. Am. Chem. Soc.* **134**, 18746–18757 (2012).
31. Behr, A. *Ullman's Encyclopedia of Industrial Chemistry* 223–269 (Wiley, Hoboken, 2010).

32. Izquierdo, J. F., Vila, M., Tejero, J., Cunill, F. & Iborra, M. Kinetic study of isobutene dimerization catalyzed by a macroporous sulphonic acid resin. *Appl. Catal. A* **106**, 155–165 (1993).
33. Kamath, R. S., Qi, Z., Sundmacher, K., Aghalayam, P. & Mahajani, S. M. Process analysis for dimerization of isobutene by reactive distillation. *Ind. Eng. Chem. Res.* **45**, 1575–1582 (2006).
34. Song, X. & Sayari, A. Sulfated zirconia-based strong solid-acid catalysts: recent progress. *Cat. Rev.* **38**, 329–412 (1996).
35. Himmel, D., Goll, S. K., Leito, I. & Krossing, I. A unified pH scale for all phases. *Angew. Chem. Int. Ed.* **49**, 6885–6888 (2010).
36. Viggiano, A. A., Henchman, M. J., Dale, F., Deakyne, C. A. & Paulson, J. F. Gas-phase reactions of weak Brønsted bases $I^-$, $PO_3^-$, $HSO_4^-$, $FSO_3^-$, and $CF_3SO_3^-$ with strong Brønsted acids $H_2SO_4$, $FSO_3H$, and $CF_3SO_3H$, a quantitative intrinsic superacidity scale for the sulfonic acids $XSO_3H$ (X = HO, F, and $CF_3$). *J. Am. Chem. Soc.* **114**, 4299–4306 (1992).

## Acknowledgements

This work, including the synthesis, characterization and crystal structure analysis, was funded by BASF SE and the US Department of Defense, Defense Threat Reduction Agency (HDTRA 1-12-1-0053). Work performed at the Advanced Light Source is supported by the Director, Office of Science, Office of Basic Energy Sciences, of the US Department of Energy under Contract no. DE-AC02-05CH11231. A portion of this research used resources at the Spallation Neutron Source, a DOE Office of Science User Facility operated by the Oak Ridge National Laboratory. NMR work was supported as part of the Center for Gas Separations Relevant to Clean Energy Technologies, an Energy Frontier Research Center funded by the US Department of Energy, Office of Science, Basic Energy Sciences under Award no. DE-SC0001015. T.M.O.P. acknowledges funding from the NSF Graduate Research Fellowship Program. C.Y. acknowledges support from a Hewlett-Packard Stanford Graduate Fellowship. P.U. acknowledges the German Research Foundation (DFG, PU 286/1-1). M.J.K. is grateful for financial support through the German Research Foundation (DFG, KA 4484/1-1). We acknowledge B. Rungtaweevoranit for his assistance with electron microscopy, and S. Teat and L. McCormick for the synchrotron X-ray diffraction data acquisition support at beamline 11.3.1 of the Advanced Light Source, Lawrence Berkeley National Laboratory.

## Author contributions

C.A.T. and T.M.O.P. co-wrote the manuscript. C.A.T. performed the PND modelling, single-crystal X-ray diffraction and PXRD experiments. T.M.O.P. performed the solid-state NMR experiments and NMR DFT calculations, with support and advice from J.A.R. J.S., Q.L. and J.B. performed the dimerization catalysis experiments with the support and advice of G.S. C.Y. performed the infrared experiments. J.W. performed the DFT calculations on the cluster models, with support and advice from M.P.H.-G. A.H. performed the PND experiments. P.U. performed the PXRD Rietveld refinements. M.J.K. helped with the thermogravimetric analysis experiments. J.J. supported and advised the synthesis. O.M.Y. supervised the project. All the authors reviewed and edited the manuscript and contributed to useful discussions.

## Competing interests

The authors declare no competing interests.

## Additional information

**Supplementary information** is available for this paper at https://doi.org/10.1038/s41557-018-0171-z.

**Reprints and permissions information** is available at www.nature.com/reprints.

**Correspondence and requests for materials** should be addressed to O.M.Y.

**Publisher's note:** Springer Nature remains neutral with regard to jurisdictional claims in published maps and institutional affiliations.